Photoinjector beam quality improvement by shaping the wavefront of a drive laser with oblique incidence*

HE Zhi-Gang(何志刚)[1)] WANG Xiao-Hui(王晓辉) JIA Qi-Ka(贾启卡)

National Synchrotron Radiation Laboratory, University of Science and Technology of China, Anhui 230029, China

Abstract: To increase the quantum efficiency (QE) of a copper photocathode and reduce the thermal emittance of an electron beam, a drive laser with oblique incidence was adopted in a BNL type photocathode rf gun. The disadvantageous effects on the beam quality caused by oblique incidence were analyzed qualitatively. A simple way to solve the problems through wavefront shaping was introduced and the beam quality was improved.

Key words: photoinjector, drive laser, oblique incidence, wavefront shaping, beam quality improvement

PACS: 29.25.Bx, 29.27.Ac, 42.60.Jf **DOI:** 10.1088/1674-1137/36/6/014

1 Introduction

X-ray free electron lasers (X-FELs) require short, high-brightness electron bunches that are typically obtained from a photoinjector. The minimum wavelength of an X-FEL scales in proportion to $\epsilon_{\rm n}/\gamma$, where $\epsilon_{\rm n}$ is the normalized transverse emittance and γ is the Lorentz factor. To reduce the saturation length of an X-FEL, the normalized transverse emittance and peak current should also be improved.

Generally speaking, transverse emittance is mainly contributed by three parts: thermal emittance, rf force, and linear and nonlinear space-charge force [1, 2]. The linear space-charge force can be fully recovered by beam optics [2] and the nonlinear space charge force can be suppressed by spatial and temporal laser shaping [3–7]. The transverse emittance can be improved further by using an uniform ellipsoidal beam with only linear space-charge force[8], which has been proposed and acquired by many groups [9–12]. The BNL type 1.6 cell gun, adopted widely at present, was designed to suppress the emittance induced by the rf force. Therefore, the thermal emittance becomes the limit of transverse emittance. By using a p-polarized laser at oblique incidence on the copper photocathode, an increase of QE of almost 5 times and a reduction of thermal emittance of 40% can be obtained [13]. The increase of QE is favorable for high peak current and will bring flexibility to laser shaping, because energy loss in the laser shaping process would then not be of excessive concern. Considering these advantages, oblique incidence at 67.5° to electron beam direction was adopted in the gun.

Oblique incidence has disadvantageous effects on beam quality, so oblique incidence is rarely adopted. In this paper, the disadvantageous effects induced by oblique incidence are analyzed qualitatively. A simple way to eliminate them is introduced and an ideal improvement of beam quality is achieved.

2 Oblique incidence & wavefront shaping

Figure 1 is the schematic diagram of the oblique incidence. If the laser spot is round, two problems will be induced: an elliptical spot on the photocathode and asynchrony of the time for the laser wavefront to reach the photocathode (time delay in the wavefront). The diameter in the horizontal (X) direction of the laser spot is extended by Ω times:

$$\Omega = 1/\cos\theta_0 = 2.6, \tag{1}$$

Received 31 August 2011, Revised 22 September 2011

∗ Supported by Science Foundation of Ministry of Education of China ("985 project": 173123200402002)

1) E-mail: hezhg@ustc.edu.cn

where $\theta_0 = 67.5^\circ$ is the angle of incidence to the electron beam direction and the diameter in the vertical (Y) direction keeps unchanged. The time delay is:

$$\tau = R_{x0} \cdot \tan\theta_0 / c, \tag{2}$$

where R_{x0} is the diameter in the X direction of the laser spot in front of the photocathode, and c is the velocity of light.

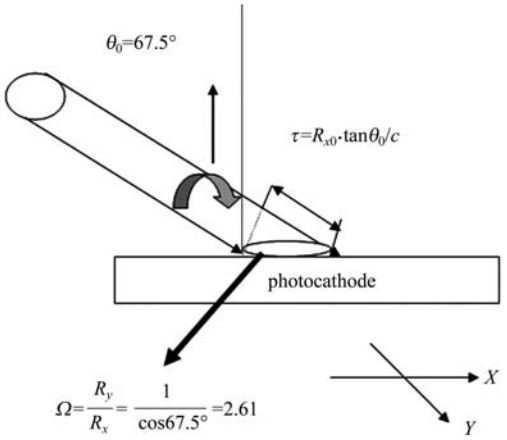

Fig. 1. Schematic diagram of oblique incidence.

The time delay will extend the pulse width and change the temporal distribution state of the electron pulse emitted from the photocathode. Fig. 2 and Fig. 3 show the changes of temporal distribution state for a gaussian pulse whose full width at half maximum (FWHM) is 10 ps, and a uniform pulse with a width of 10 ps, respectively. This change is not acceptable for uniform pulses.

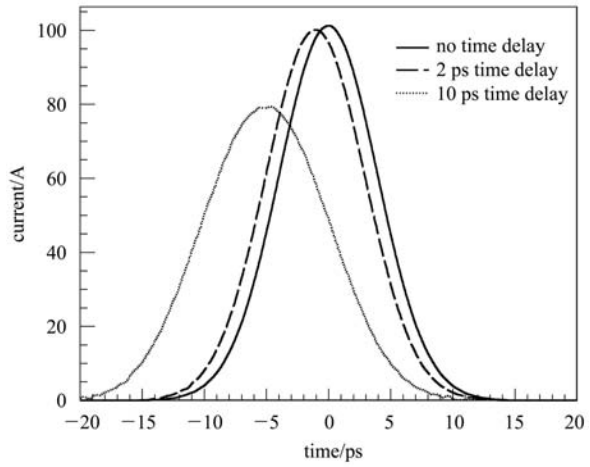

Fig. 2. Current distributions of a Gaussian pulse at different time delays.

To correct the elliptical spot on the photocathode and the time delay of the wavefront, a simple set of wavefront shaping optics, which is shown in Fig. 4, was inserted in the optical transport line.

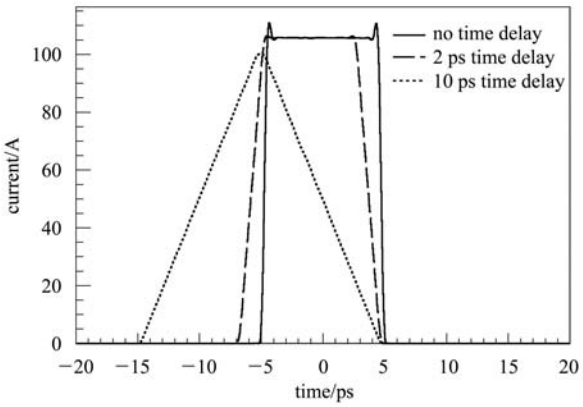

Fig. 3. Current distributions of an unform pulse at different time delays.

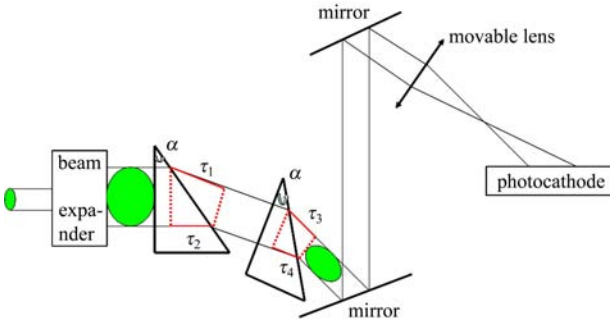

Fig. 4. Diagram of wavefront shaping.

Two prisms were used to generate negative ellipticity and time delay to correct the ellipticity and time delay caused by oblique incidence. The negative ellipticity caused by the prisms is:

$$\Omega' = 1 - n^2 \sin^2\alpha / \cos^2\alpha. \tag{3}$$

For a monochromatic light, the time delay brought by the prisms is:

$$\tau' = \tau_1 - \tau_2 + \tau_3 - \tau_4 = R_x(n-1)\cdot\tan\alpha \cdot\left(1+\sqrt{1-n^2\sin^2\alpha}/\cos\alpha\right), \tag{4}$$

where α is the angle of the prisms (about 35°), $n = 1.5$ is the refractive index of the quartz for UV light with a wavelength of 262 nm, and R_x is the diameter in the X direction of the laser spot on the surface of the first prism. Because the prisms are dispersive elements, there is a pulse front tilt for a short laser pulse to illuminate them [14]. Therefore, a further negative time delay can be acquired, but it is minute. The original and reshaped UV laser profiles in front of the photocathode are shown in Fig. 5.

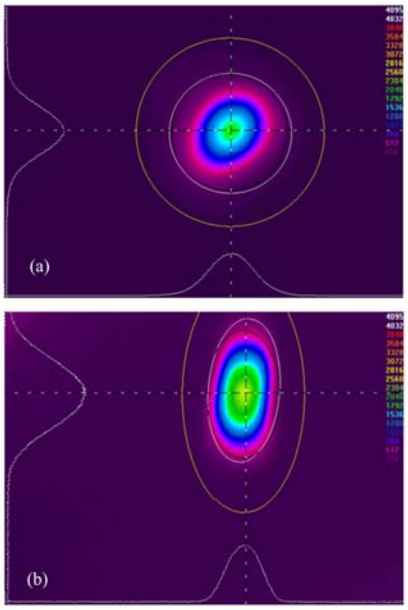

Fig. 5. Laser profiles in front of the photocathode. (a) Without shaping; (b) with shaping.

The diameters of the laser spot without and with wavefront shaping are shown in Table 1, where R_{x0}, R_{y0}, R_{xc} and R_{yc} are the diameters in X and Y directions of the laser spot in front of and on the photocathode, respectively. R_x is chosen to be $R_x = 4.4$ mm, so τ' is about 6 ps calculated from Eq. (4), and τ was about 9.6 ps calculated from Eq. (2). If a variable beam expander is used, R_x can be tunable, then τ' can also be tunable.

Table 1. Diameters of the laser spot (unit: mm).

	R_{x0}	R_{y0}	R_{xc}	R_{yc}
without wavefront shaping	1.8	1.9	4.68	1.9
with wavefront shaping	1.1	2.1	2.86	2.1

3 Emittance evolution and improvement through wavefront shaping

For a gun with drive laser at oblique incidence, the transverse emittances in the X and Y directions are influenced by three factors: the increase of diameter in the X direction, the decrease of charge density caused by the increase of transverse area and the coupling effect. In an rf gun, the transverse emittance in the X direction increases dramatically because of the increase of diameter in the X direction. As the charge density decreases, the growth of transverse emittance in the Y direction can be suppressed, but it is also affected by the coupling effect from the X direction. Electrons are rearranged in the compensation solenoid. The evolution of transverse emittances in X and Y directions depends on the microwave electric field strength, the compensation solenoid magnetic field strength, and the acceleration phase. It can be predicted that the emittances in two directions obtained by a round spot with oblique incidence on the photocathode would increase.

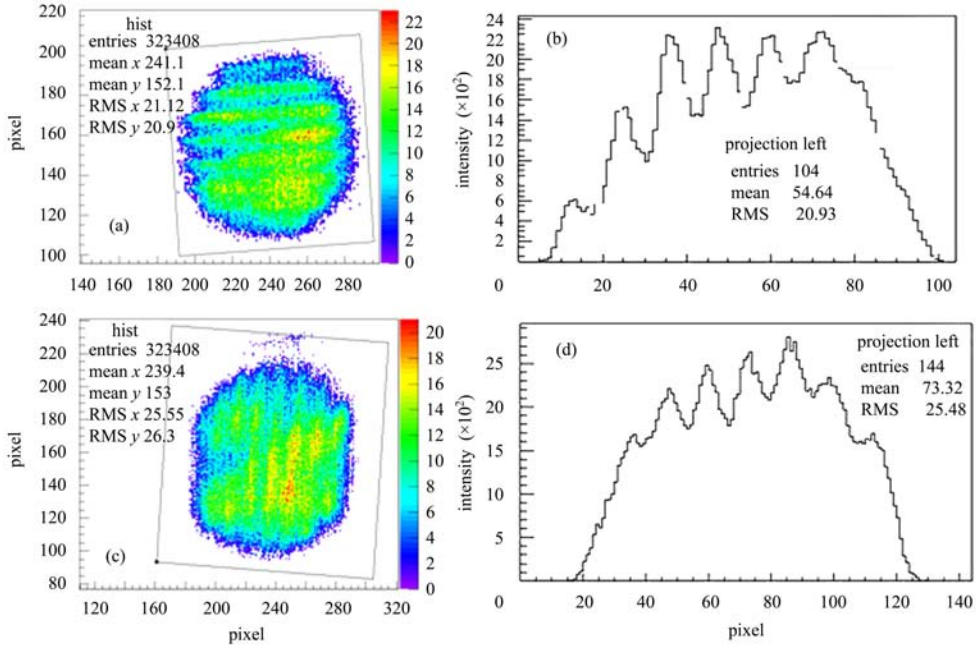

Fig. 6. (a) False color image of the beam passing through the horizontal slits; (b) intensity graph found by summing the horizontal pixel values at a given vertical position; (c) false color image of the beam passing through the vertical slits; (d) intensity graph created by summing the vertical pixel values at a given horizontal position.

Table 2. The measured transverse emittances (unit: mm·mrad).

Max B_z & wavefront shaping state	ϵ_x	$\epsilon_x^{\rm n}$	ϵ_y	$\epsilon_y^{\rm n}$
792 Gauss & without wavefront shaping	1.49	7.86	1.24	6.50
792 Gauss & with wavefront shaping	1.04	5.47	0.92	4.85
826 Gauss & without wavefront shaping	1.24	6.50	1.02	5.30
826 Gauss & with wavefront shaping	0.91	4.78	0.79	4.17

The transverse emittance was measured by multi-slits technique [15]. The slits are spaced 1 mm from each other, with a width of 90 μm each. The multi-slit was set at a distance of 0.55 m downstream from the the cathode, and the beamlet profile was measured by using a YAG crystal screen at a distance of 1.05 m downstream from the cathode. The measured false color images with the slits and intensity graphs found by summing the horizontal and vertical pixel values at a given vertical and horizontal position are shown in Fig. 6. The zoom factor of the camera is about 0.0845 mm per pixel.

The widths of the slits are so wild that the slits in the beam image could not be resolved enough for a small beam to pass through them. If a beam is too large, the image would be out of the range of the YAG crystal screen. Therefore, only two groups of emittances were measured.

When the maximum magnetic field strengths of the compensation solenoid (Max B_z) were 792 Gauss and 826 Gauss, the geometrical emittances in X and Y directions (ϵ_x and ϵ_y) were measured, as shown in Table 2.

Although the electron beam energy cannot be measured yet, it can be estimated by the measured microwave power, which is about 4 MW. A maximum acceleration gradient of approximately 60 MV/m could be obtained using our gun; an average energy of 2.7 MeV was gained by ASTRA [16] simulation. Therefore, the normalized transverse emittances in the X and Y directions ($\epsilon_x^{\rm n}$ and $\epsilon_y^{\rm n}$) were estimated by the average energy, as shown in Table 2. The transverse emittances in the X and Y directions were improved by wavefront shaping, and the differences between the emittances in two directions were decreased. In addition, the beam charge was measured to be about 0.17 nC (about the energy of 40 μJ UV laser illuminated on the cathode) by using an integrating current transformer (ICT).

The transverse emittances at the distance of 0.55 m downstream from the cathode without and with wavefront shaping were also simulated using the measured parameters, when the maximum magnetic strengths of the solenoid were 792 Gauss and 826 Gauss.

Figure 7 shows the simulation results when the maximum magnetic strength of the solenoid was 826 Gauss. The measured results correspond to the simulated results when the acceleration phase is smaller than 35 degrees. The measured emittances are higher than the simulation results. That might come from the thermal emittance, which is not included in the simulation, emittance measurement error and an error in finding the maximum magnetic strength of the solenoid. Furthermore, the transverse emittances in two directions would increase dramatically for a 1 nC charge beam in a gun with a 100 MV/m maximum acceleration gradient and a round laser spot at oblique incidence. The average emittances in two directions is increased by several times. For that case, the emittance improvement caused by wavefront shaping can be more notable.

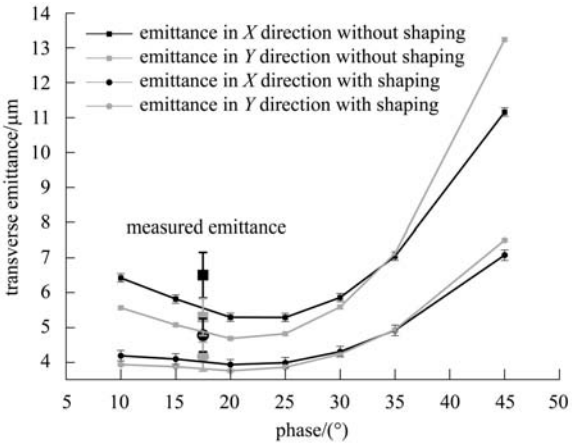

Fig. 7. Simulation and measured results of emittance. Black: emittance in the X direction; gray: emittance in the Y direction; square: without wavefront shaping; circle: with wavefront shaping.

4 Improvement of the temporal pulse distribution

As mentioned in Part 2, the time delay extended the pulse width, which caused the increase of energy spread and the narrowing of the phase range without back bombardment. Beam charge was measured at

relative phases, which was induced by a phase shifter, as shown in Fig. 8.

The phase width without back bombardment was expanded by wavefront shaping. The energy spread should also be diminished. However, the instruments required for energy spread measurement had not yet been installed. To avoid possible damage to the cathode caused by back bombardment, only several points were measured.

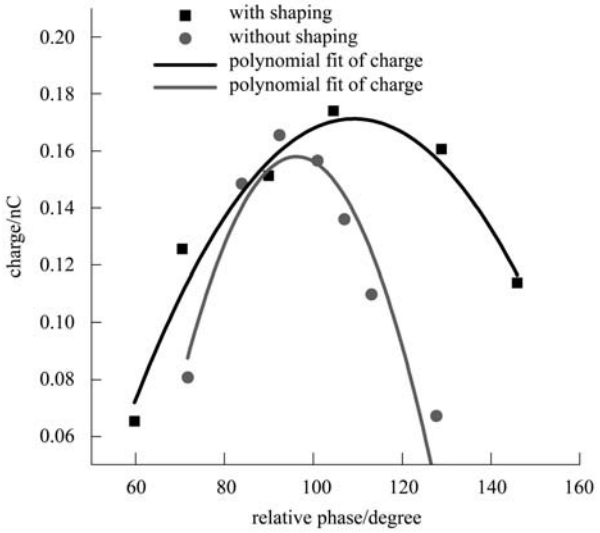

Fig. 8. Beam charge vs relative phase (with and without wavefront shaping).

5 Compatibility of wavefront shaping and spatial shaping

A pi-shaper [17] sample was used to reshape the spatial distribution of the UV laser spot. The laser profiles at the back of the shaper and the wavefront shaping optics are shown in Fig. 9. The primary results prove that the wavefront shaping and spatial shaping are compatible. In addition, an image relay system should be designed to transport the reshaped laser profile to the photocathode. The relevant experiment was broken down by the grievous shutdown of the laser system.

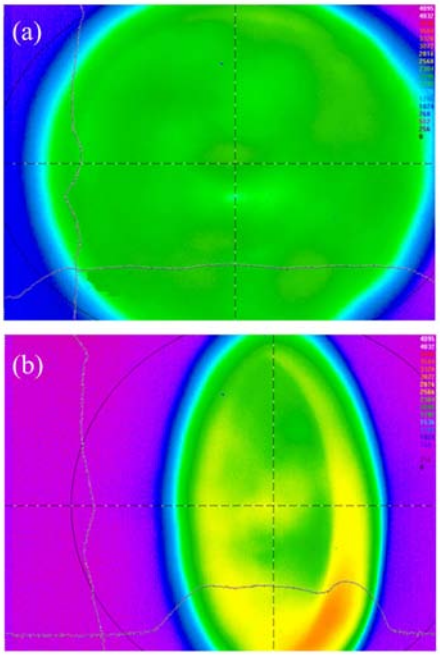

Fig. 9. (a) Laser profile at the back of the pi-shaper; (b) Laser profile at the back of the pi-shaper and wavefront shaping optics.

6 Conclusion

Simple wavefront shaping optics were inserted in an optical transport line to eliminate the problems caused by oblique incidence. Improvements of transverse emittance and the temporal pulse distribution state were achieved. The disadvantages of oblique incidence can be corrected completely by wavefront shaping. The primary results of laser shaping, aiming to generate a uniform spatial spot on the photocathode, were not affected by wavefront shaping.

References

1 Carlsten B E. Nucl. Instrum. Methods A, 1989, **285**: 313
2 Kim K J. Nucl. Instrum. Methods A, 1989, **275**: 201
3 Tomizawa H, Dewa H, Taniuchi T et al. Nucl. Instrum. Methods A, 2006, **557**: 117
4 SharmaA K, Tsang T, Rao T. Phys. Rev. ST Accel. Beams, 2009, **12**: 033501
5 LIU Sheng-Guang, Masafumi F, Sakae A et al. CPC (HEP & NP), 2010, **34**(5): 584
6 YANG J, Sakai F, Yanagida T et al. J. Appl. Phys., 2002, **92**(3): 1608
7 Weiner A M. Rev. Sci. Instrum, 2000, **71**: 1929
8 Limborg-Deprey C, Bolton P R. Nucl. Instrum. Methods A, 2006, **557**: 106
9 Luiten O J, Van der Geer S B, Loos M J et al. Phys. Rev. Lett., 2004, **93**: 094802
10 Claessens B J, Van der Geer S B, Taban G et al. Phys. Rev. Lett., 2005, **95**: 164801
11 Musumeci P, Moody J T, England R J et al. Phys. Rev. Lett., 2008, **100**: 244801
12 LI Y L, Lewellen J W. Phys. Rev. Lett., 2008, **100**: 074801
13 XIANG D, Park S J, Park J H et al. Nucl. Instrum. Methods A, 2006, **562**: 48
14 Hebling J. Optical and Quant Electronics, 1996, **28**: 1759
15 Anderson S G, Rosenzweig J B. Phys. Rev. ST Accel. Beams, 2002, **5**: 014201
16 Flottmann K. ASTRA user manual, http://www.desy.de/~mpyflo/
17 http://www.pishaper.com/index.html